RESEARCH ARTICLE

INTERNATIONAL RESEARCH JOURNAL OF MULTIDISCIPLINARY TECHNOVATION

Asian Research Association

DOI: 10.54392/irjmt2454

Modelling of Restrained Shrinkage Stresses in Mortar using Artificial Neural Networks

Miriam W. Njoroge [a,*], Silvester O. Abuodha [b], Erastus K. Kabando [a], Kevin O. Achieng [a]

[a] Department of Civil Engineering, Dedan Kimathi University of Technology, Nyeri 10143, Kenya
[b] Department of Civil and Construction Engineering, University of Nairobi, Nairobi 00100, Kenya
*Corresponding Author Email: njorogewacu@gmail.com
DOI: https://doi.org/10.54392/irjmt2454
Received: 04-01-2024; Revised: 23-08-2024; Accepted: 15-09-2024; Published: 18-09-2024

Abstract: Accurate prediction of tensile stresses in repair mortars is vital for the long-term durability of rehabilitated concrete structures. Existing analytical models are based on the material property theory and often struggle to capture the intricate and non-linear behavior exhibited by different mix types used in concrete. To address the limitation of existing models, neural networks were employed as a modelling approach for more robust and versatile predictions. The data used in developing the models was obtained from laboratory experiments. The input variables to the ANN model included: water content, cement, silica fume, superplasticizer, admixture, and age. Three distinct ANN-based models were developed based on: ordinary Portland cement, 10% silica fume as a partial replacement of cement and a combination of the two binder types. These models were evaluated using four performance metrics: coefficient of determination (R2), root mean square error (RMSE), mean absolute error (MAE), and mean absolute percentage error (MAPE). When mortars with ordinary Portland cement was used as a binder, the R2, MAE, MAPE, and RMSE were 99.74%, 0.0808, 0.0397, and 0.0138, respectively. For mortars with 10% silica fume, the ANN model predicted restrained shrinkage stresses in mortars with R2, MAE, MAPE, and RMSE values of 99.25%, 0.0090, 0.0731, and 0.3161, respectively. When both binders were used, the R2, MAE, MAPE, and RMSE were 99.77%, 0.0093, 0.0804, and 0.1775, respectively. The application of neural networks for predicting restrained shrinkage stresses in repair mortars outperforms conventional models with enhanced accuracy and reliability. The developed ANN models serve as powerful tools for assessing and optimizing the performance of repair mortars, enabling more efficient and precise design strategies in concrete repair.

Keywords: Artificial Neural Networks, Restrained Shrinkage Stresses, Concrete Repair, Elastic modulus, Drying shrinkage

1. Introduction

Concrete can be defined as a composite material consisting of a binding medium and coarse granular materials [1]. It has been extensively utilized in constructing diverse infrastructures for over a century, owing to its durability and high structural capacity. However, despite its advantages, concrete structures undergo deterioration and a subsequent decrease in their structural capacity, resulting in a reduced service life. To address this issue, government institutions and private organizations worldwide allocate budgets for costs associated with the repair and rehabilitation of deteriorated structures [2].

The construction industry, therefore, has two options: either design or construct structures that require minimal maintenance or repair or develop ways for rehabilitation, repair, and protection of the existing deteriorated concrete structures to maintain the designed service life [3]. The recommended technique for the repair and rehabilitation of concrete structures is bonded concrete overlay [4]. This technique is economically viable and involves the removal of the deteriorated concrete surface followed by the placement of a fresh concrete layer, commonly referred to as a patch repair. The bonded concrete overlay is particularly used for repairing deteriorated surfaces, offering an effective and efficient solution to address structural issues.

Despite technological advancements, failure analysis in repair projects has revealed that bonded concrete overlays often underperform due to issues like cracking and debonding, leading to premature failure [5]. Several factors contribute to this failure, including poor workmanship, extreme weather conditions, and misdiagnosis of the original cause of failure. The

performance of bonded overlays is influenced by both internal and external loading, including external restraints, structural loads, volume deformations, and chemical reactions. Hydrostatic loads primarily cause volume deformations in the overlays due to water expulsion from the calcium silicate gel [6]. The bond between the overlay and substrate creates external restraints, resulting in bending stresses, uniaxial stresses, interface shear, and tensile stresses [7, 8]. When the tensile stresses exceed the tensile strength of the concrete, the overlay cracks [9]. Cracking in concrete leads to the ingress of chlorides and sulfates that cause corrosion and further deterioration of the structure, affecting durability and serviceability requirements [10, 11]. It is crucial to address these factors during the design and implementation of bonded concrete overlay repairs to ensure long-term effectiveness and performance of the repaired structures.

Crack initiation in overlays is influenced by various material properties of the mortar, including elastic modulus, tensile relaxation, tensile strength, and drying shrinkage. The relationship between these material properties determines crack propagation behavior. Researchers have observed that an increase in drying shrinkage and elastic modulus, along with a decrease in tensile strength and tensile relaxation, raises the risk of cracking in restrained concrete. Tensile relaxation is a crucial mechanism for stress relief in mortars, capable of alleviating up to 60% of the restrained shrinkage stresses [12]. Understanding the mechanisms of tensile relaxation is vital for reducing the development of restrained shrinkage stresses and achieving efficient stress prediction [13].

Proper mix design is crucial for controlling the development of restrained shrinkage stresses by carefully considering the material properties of concrete. The addition of fibers, such as polypropylene and cellulose, has been observed to mitigate plastic shrinkage in cement-based materials. For instance, sisal fibers have shown effectiveness in reducing plastic shrinkage and controlling early-age concrete cracking [14]. Moreover, incorporating supplementary cementitious materials like silica fume, limestone powder cement, ground granulated blast furnace slag, and fly ash can enhance the mechanical properties of concrete. This enhancement contributes to increased resistance against cracking and restrained shrinkage stresses.

Notably, using fly ash and metakaolin as partial cement replacements reduces porosity through the formation of carbon aluminate which may decrease drying shrinkage by 30% primarily through the formation of carbon aluminate, consequently decreasing drying shrinkage. This reduction directly impacts the development of restrained shrinkage stresses, thus delaying cracking [15]. Silica fume, characterized by its highly reactive nature due to its small particle size is predominantly composed of SiO_2. It is typically added in small amounts approximately 5-10% to mitigate bleeding and enhance mechanical properties. It has a role in accelerating the hydration kinetics of the cement paste by providing nucleation sites for the hydration process to occur also known as the filler effect which does not interfere with the chemical reactions of the cement paste [16]. Expansive agents like aluminum powder have shown significant promise in reduction of drying shrinkage and reduction of crack widths in mortar. The formation of ettringite in small quantities is beneficial due to the filling of the pores, resulting in a denser matrix and therefore improved mechanical properties [17].

The commonly used method for combating tensile stresses is to increase the tensile strength of the mortar mixes by reducing the water content. The reduction in water content leads to a higher elastic modulus and a reduction in tensile relaxation which is the main stress relief mechanism [18]. It is therefore crucial to have adequate knowledge on the effect of each mix design parameter or material when designing mortars that might experience restrained shrinkage stresses.

To address this complexity and enhance the understanding of restrained shrinkage stress development, there arises a pressing need to develop a machine-learning model capable of being trained on input parameters and accurately predicting the evolution of restrained shrinkage stresses. Such a model could revolutionize the field of concrete engineering, offering advanced tools for optimizing mix designs and ensuring the long-term durability and performance of rehabilitated structures.

1.1 Existing Models for the Prediction of Restrained Shrinkage Stresses in Mortar

Various methods have been employed to predict restrained shrinkage stresses in bonded overlays, including the prestress analogy, localized strain theory, and material property theory. The simple beam theory, based on the prestress analogy, relies on certain assumptions: plane sections remain plane after bending, force transfer occurs at member ends, complete restraint exists between the substrate and the overlay, and the model converts internal stresses to external stresses to predict tensile stresses [19, 20]. An example of a model developed using the prestress analogy is the Silferbrand model [21] represented in Equation (1).

$$\sigma(t) = \mu E(t)^{*}\varepsilon_{sh}t) \quad (1)$$

$$\mu = \frac{m(1-\alpha)\{m(1-\alpha^3)+\alpha^2(3+\alpha)\}}{m+(m-1)\{m(1-\alpha^4)-\alpha^4\}} E(t)^{*}\varepsilon_{sh}t) \quad (2)$$

$$E^{*} = \frac{E_1}{1+\emptyset(t)} \quad (3)$$

$$m = \frac{\text{modulus of elasticity of the substrate } E_2}{\text{modulus of elasticity of repair material } E^{*}} \quad (4)$$

Where; ε_{sh}t-shrinkage of the overlay, E^*-elastic modulus of the repair material,μ-degree of restrain, $\emptyset(t)$-coefficient of creep,α-ratio of the total depth of repair to the substrate depth. The elastic modulus is calculated by incorporating the effect of creep as shown in (Equation 3) Baluch [22]. based the differential shrinkage model on the beam theory by assuming that tensile stresses were not affected by substrate rigidity as shown in Equation (5)**Error! Reference source not found.**, where E(t)-elastic modulus of repair material ,$\varepsilon_{sh}(t)$-Total strain in the repair material,$\sigma(t)$-Shrinkage stresses in the repair material.

$$\sigma(t) = \frac{E(t)\varepsilon_{sh}(t)}{(1+E_C(t)} \quad (5)$$

The material property theory and the localized strain theory calculate restrained shrinkage by determining the product of concrete stiffness, free strain, and degree of restraint [23]. The degree of restraint is defined as the ratio of the actual stress to the full stress if the repair was fully bonded. Localized strain theory is based on the following assumptions: shrinkage along the depth of the overlay is assumed to be constant and the bond between the overlay and the substrate is assumed to be perfect resulting in full strain compatibility between the overlay and the substrate interface [4]. Differential shrinkage stresses are calculated from the sum of interface strains as expressed in Equation (6). The model is based on the superposition of instantaneous creep and creep strain. The calculation for creep strain is shown in Equation (7) and instantaneous strain in Equation (8).

$$\varepsilon_{total}, I(t) = \varepsilon_{insta}, I(t) + \varepsilon_{creep}, S, I(t) \quad (6)$$

$$\varepsilon_{creep}, S, I(t) = \varepsilon_{insta}, I(t) * 0.8 * \varphi_s(t, t_o) \quad (7)$$

$$\varepsilon_{insta}, I(t) = \varphi_s(t, t_o).\varepsilon_{FSS}.\frac{1}{1+\frac{E_S}{E_O(t)}.C_e+0.8.\varphi_s(t,t_o)} \quad (8)$$

Where: $\varepsilon_{total}, I(t)$-total strain , $\varepsilon_{creep}, S, I(t)$- creep strain,$\varepsilon_{insta}, I(t)$-strain producing stress in the substrate(instantaneous strain), $\varphi_s(t, t_o)$ – coefficient of tensile relaxation, ε_{FSS}-free shrinkage strain the overlay, C_e-Coefficient explaining the influence of member dimensions and strain profile and $\varphi_s(t, t_o)$ -tensile relaxation function of the overlay. The elastic properties of the overlay, overlay relaxation function and substrate need to be measured or estimated. The substrate and the overlay materials determine the empirical constant Ce which is estimated as 1 in the localized strain theory model.

$$\sigma(t) = \left(1 - \frac{\varphi}{100}\right).(\alpha.\varepsilon_{FSS}).E_O \quad (9)$$

The model developed by Silferbrand [24] was adopted by Carlsward [24] by increasing the number of steps in calculating tensile stresses from one step to incremental steps. Kristiawan [25] proposed the use of the model shown in Equation (10) to predict tensile stresses, where σ(t)-Tensile stresses and ε_sh-shrinkage stresses.

$$\sigma(t) = 0.0093\varepsilon_{sh} \quad (10)$$

1.2 Limitation of the Existing Analytical models

The existing material property model was originally formulated based on traditional concrete materials like water, binder, and aggregates. However, advancements in admixtures and cement extenders have arisen, necessitating a need for reassessment of the model. Additionally, incorporating modern concrete technology for crack prevention, such as the inclusion of rubber particles to enhance flexibility, internal curing techniques, optimized aggregate contents, and intelligent use of cementitious binders, is crucial for improving the model's accuracy and relevance [26].To address these challenges and enhance the understanding of bonded overlays, the current research aims to utilize machine learning techniques to develop a robust and adaptable model that can account for changes in mix design parameters in mortars.

The primary focus of this research is on employing machine learning models, particularly Artificial Neural Networks (ANNs), to predict restrained shrinkage stresses in mortar. The effects of variations in water content, supplementary cementitious materials, binder content, use of superplasticizer, shrinkage compensating admixture, and the influence of age will be considered in the modeling process. By utilizing ANN-based predictive models, this research aims to significantly advance our understanding of tensile stress development and ultimately improve the effectiveness and durability of repair strategies in concrete engineering.

2. Research Significance

The repair and rehabilitation of deteriorated structures is a challenge to economies globally due to early age cracking of the repair which not only is aesthetically unpleasing but also causes further deterioration of the structure [11]. The study compliments efforts by other researchers to improve the material property model that predicts the development of restrained shrinkage stresses which is the main cause of cracking in patch repairs. The study of the properties and behavior of materials used in repairs allows engineers working in the field of repair to perform life cycle management of the structures [27]. The research provides a comprehensive analysis of crucial factors, such as water content, binder content, age, supplementary cementitious materials, and superplasticizer, which are vital in the development of repair mortars. With the continuous advancements in admixtures, such as shrinkage-reducing admixtures, shrinkage compensating admixtures, and super absorbent polymers, it is essential for repair contractors and engineers to stay updated on material behavior and

properties, warranting the need to update existing techniques and models. A study on the field effectiveness of repair mortars revealed that 60% of the repairs failed by cracking on the overlay surface,45% failed by cracking due to drying shrinkage leading to carbonation attack;40% of the cracked surfaces rapidly deteriorated increasing the depth of carbonation and affecting reinforcements [28]. The American Society of Civil Engineers estimated the cost of repair and rehabilitation of structures to be $18 to $21 billion in the United States in 2009 [29]. While the costs of rehabilitation are substantial, the costs of a poorly executed design are higher. Governments spending money for rehabilitation means that funding for other sectors of the economy such as education, food, and healthcare is reduced. The cracking of concrete affects the appearance, water tightness, and functionality of buildings. It is therefore important for repair engineers and contractors to have a proper understanding of the material properties of repair mortars for effective repairs.

The incorporation of machine learning techniques in the civil engineering industry is crucial to improving design reliability. In prediction of restrained shrinkage stresses as compared to other methods, the neural network is able to learn the complex relationships between the variables and produce a robust and versatile model. This was done by identifying the most critical material parameters and their interactions with restrained shrinkage stresses through heatmaps (Pearson correlation coefficients). The technique used in prediction not only saves time and money but also offers better accuracy in terms of versatility and robustness. This can accelerate the application of construction materials in the field and reduce the time taken when conducting experiments.

3. Methods

3.1 Materials and Test Methods

The materials used in the research are Ordinary Portland Cement 42.5 N, Silica fume, Shrinkage compensating admixture from Forsroc, River sand, and Superplasticizer from Sika.

3.1.1 Ordinary Portland Cement

Ordinary Portland cement (42.5N) was used in the research. Ordinary Portland Cement is versatile, available and affordable and is used majorly in the construction industry [30]. It also offers an infinite variety of applications and offers optimal performance in ambient temperature in the life cycle of a building. The research chose Ordinary Portland cement as despite its numerous advantageous, cement mortars made from OPC which is the most common cement used have a weak cracking resistance, low deformability and low bending resistance as compared to other mechanical properties such as compressive strength.

3.1.2 Supplementary Cementitious Material

Silica fume is produced as a byproduct of production of ferrosilicon alloy production it was used in this study and obtained from Bale mining with 93.35% SiO2 content which was sufficient to produce a pozzolanic reaction. A study by Megat *et al.* [31] observed that other SCMs such as fly ash and ground granulated blast furnace slag reduced the early age strength of concrete, but long-term age was increased [32, 33]. While checking the early age cracking of materials, silica fume was chosen as an alternative. The chemical properties of the silica used is as shown in Table 1.

3.1.3 Fine Aggregates

Natural river sand used had a fineness modulus of 2.09 with a density of 2690 kg/m^3. The gradation curve is as seen in Figure 1. With aggregate sizes ranging from 4.75mm to 0.15 microns. The gradation lies between the maximum and the minimum values as outlined in ASTM C136 The aggregate to cement ratio was constant and maintained at 1:3 with the weight of cement [34].

3.1.4 Superplasticizer

Superplasticizer used in the research was Sika Visocrete-2100 which is a high range water reducing admixture. The admixture meets the requirements defined by ASTM C494.The percentage used in the research was determined through trial tests to be 0.042%. The percentage to be used in the experiment was determined through trial tests.

3.1.5 Shrinkage Compensating admixture

Cebex 100 was used as the shrinkage compensating admixture. Its plasticizing and expanding action and conform to BS 8110 Part 1:1985 [35]. The plasticizing effect allowed the increase of workability and the expansion reduced settlement and shrinkage. Cebex 100 was chosen due to its compatibility with all types of cement.

Table 1. Physical Properties of Silica Fume

	SiO_2	AL_20_3	CaO	MgO	Na20	K_20	TiO_2	MnO	Fe_20_3	LOI	Moisture
Silica fume	93.35	1.83	0.11	1.22	0.40	0.83	0.24	0.01	0.13	0.28	0.19

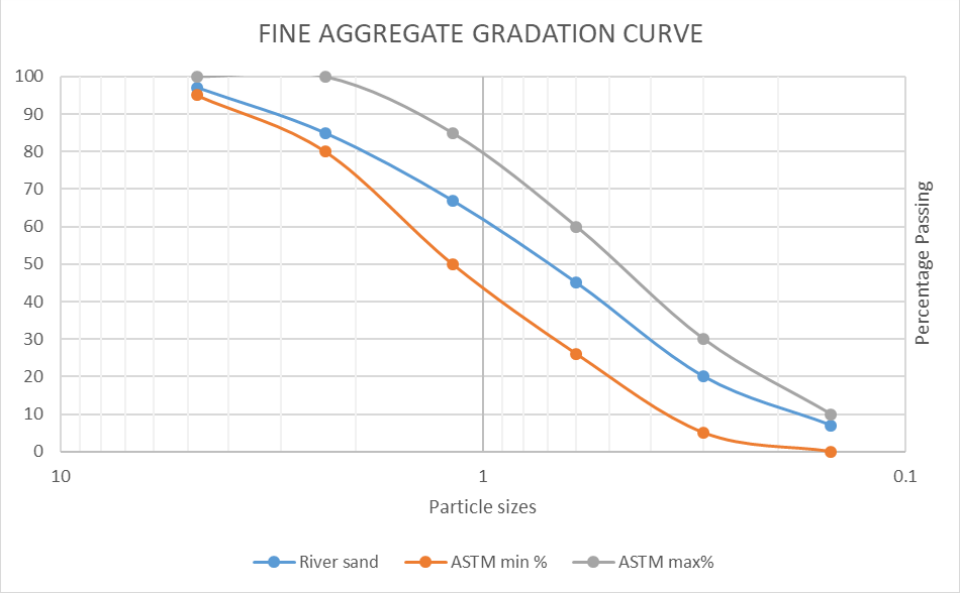

Figure 1. Gradation of Fine aggregate according to ASTM C136

3.1.6. Water to cement ratios

The water to cement ratios used in the research were 0.45,0.55 and 0.65 to represent low w/c ratio. medium w/c ratio and a high-water cement ratio. The 10% partial replacement with silica fume was determined from a trial mix design and justified with literature sources. The percentage in weight of superplasticizer used in the experiment was determined from trial mixes in the laboratory. The percentage of Shrinkage compensating admixture was determined from manufacturers specifications. The research had 12 trial mixes as shown in Table 2 and tested for 28 days.

3.2 Experimental tests

3.2.1 Elastic Modulus

The Elastic Modulus test was conducted on cylindrical specimens of 150mm diameter and 300 mm height by applying a compressive load as outlined in BS 1881: Part 121:1983 [36]. The loading rate of the Universal testing Machine was 0.6Mpa/s and the specimen were loaded until the stress was equal to a third of the compressive strength of the specimens. The static elastic modulus was calculated at 3, 7, 14, 21 and 28 days.

3.2.2 Drying shrinkage

The drying shrinkage test was conducted according to ASTM C157-75 [37]. The change in length of 285*40*40 mm specimens were taken using a length comparator daily. Three specimens were prepared for every sample. The shrinkage strain was calculated as shown in Equation (11). Where L_O is the initial length, L_I is the length at measured daily and ε_{dr} is the drying shrinkage strain.

$$\varepsilon_{dr} = \frac{L_I - L_O}{L_O} \quad (11)$$

3.2.3 Tensile relaxation

Tensile relaxation has been recognized by various studies to provide a stress relief mechanism in restrained shrinkage stresses. The fib Model Code 2010 recommends the use of age adjusted effective modulus method for prediction of tensile relaxation due to the difficulty in conducting the experiment [38]. The formula used in this study is as shown in Equation (12) where $\varphi(t, t_0)$ is the coefficient of relaxation at time t, $\emptyset(t, t_0)$ is the coefficient of creep at time t, E_C is the modulus of elasticity at 28days, $E_C(t_o)$ is the modulus of elasticity at time t_o and $\aleph$ is the coefficient of aging taken as 0.8.The creep coefficient was calculated as outlined in BS EN 1992-1-1 [39].The age adjusted effective modulus method improves the efficiency as it is time saving [40].

$$\varphi(t, t_0) = \frac{\emptyset(t,t_0)}{\frac{E_C}{E_C(t_0)} + \aleph(\emptyset(t,t_0))} \quad (12)$$

3.3 Restrained Shrinkage Stresses

The response variable restrained shrinkage stresses were calculated from material property theory shown in equation (9) and the results are represented in the supplementary table 1.

3.4 Limitation of the Methods

The method used to get values for tensile relaxation is an estimation based on the age adjusted effective modulus due to the complexity in doing the actual test. However, the age adjusted effective modulus has been proven effective in estimation of the tensile relaxation values.

Table 2. Mix proportion and properties

MIX ID	w/b	Water Content (/m³)	Cement Content (Kg/m³)	Shrinkage Compensating Admixture (%by weight of cement)	Silica fume Content (Replaced 10% by weight of cement)	Superplasticizer (% by weight of cement)
1	0.45	180	400	0	0	0.42
2	0.45	180	400	0.045	0	0.42
3	0.45	180	360	0	40	0.42
4	0.45	180	360	0.045	40	0.42
5	0.55	185	336	0	0	0.42
6	0.55	185	336	0.045	0	0.42
7	0.55	185	302.4	0	33.6	0.42
8	0.55	185	302.4	0.045	33.6	0.42
9	0.65	190	292	0	0	0.42
10	0.65	190	292	0.045	0	0.42
11	0.65	190	262.8	0	29.2	0.42
12	0.65	190	262.8	0.045	29.2	0.42

4. Results and Discussion

4.1 Effect of water content on development of Restrained Shrinkage Stresses for mixes with Ordinary Portland Cement as the binder

From Figure 2, the restrained shrinkage stress reached its highest at a water-cement ratio (w/c) of 0.65, followed by 0.55, with the lowest stress observed at 0.45. This can be explained by understanding the interaction in the interfacial transition zone. In the interfacial transition zone, an increase in water content results in a coarser pore distribution, leading to an expected porosity increase of up to 150% for a w/c of 0.65 compared to mixes with a w/c of 0.45 [41]. Higher w/c ratios also increase the evaporation rates, consequently increasing shrinkage. This rise in porosity reduces the mechanical properties of mortar including elasticity. However, the reduction in stiffness is counteracted negatively by increased shrinkage, therefore increasing restrained shrinkage stresses.

During the initial five days, the 0.45 mix exhibits higher restrained shrinkage stresses compared to the 0.65 mix, attributable to a combined effect of autogenous and drying shrinkage. Although aggregate size influences the interfacial transition zone, the constant aggregate size used in this mix suggests a negligible effect. Nonetheless, larger aggregate particles are expected to retain more bleed water than smaller ones, leading to higher local water content. This increase in local water content results in decreased unhydrated cement content and higher porosity. Increase in w/c ratio increases capillary porosity, facilitating microcracking at the interfacial zone. This reduces the stiffness since the aggregate-cement interface represents the weakest link influencing the curvature in the stress-strain relationship.

4.2 Effect of silica fume on development of restrained shrinkage stresses

From Figure 3 plain mixes with only ordinary Portland cement as the binder developed the highest shrinkage stresses as compared to blended mixes. This can be attributed to the pore filling and the effect of the hydration products. Cement hydration involves a reaction between water, dicalcium silicate and tricalcium silicate resulting in the formation of portlandite (calcium hydroxide crystals and C-S-H (Calcium Silicate Hydrate).

The formation of calcium silicate hydrate affects the mechanical properties of the mortar including elastic modulus. The C-H crystals/portlandite control the Ph by forming a passive layer and controlling corrosion [42]. Silica fume reacts with portlandite to form secondary C-S-H leading to increase in alkali and changing the pore structure [16]. The additional C-S-H reduces the pores and increases the stiffness of the mortar. The mixes with silica fume have reduced restrained shrinkage stresses due to the increase in resistance to the deformation of concrete materials which can be explained by the bridge formed by the silicon tetrahedron between the gel chain and the silicon dimers.

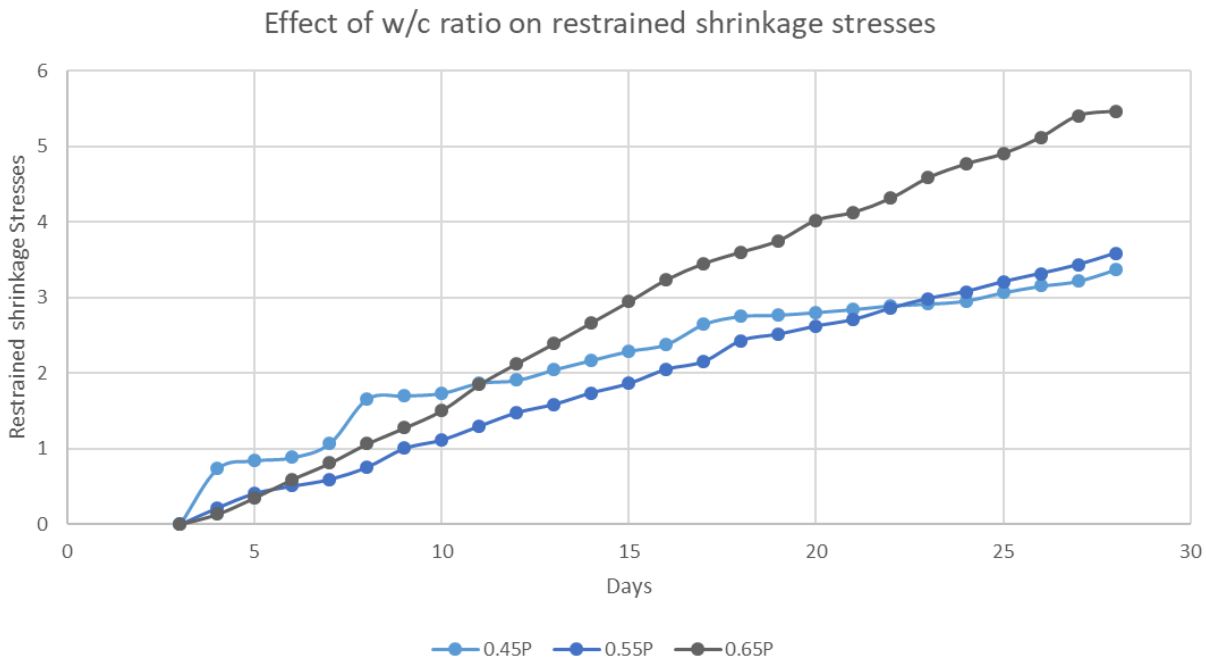

Figure 2. Effect of w/c ratio on Development of Restrained Shrinkage Stresses

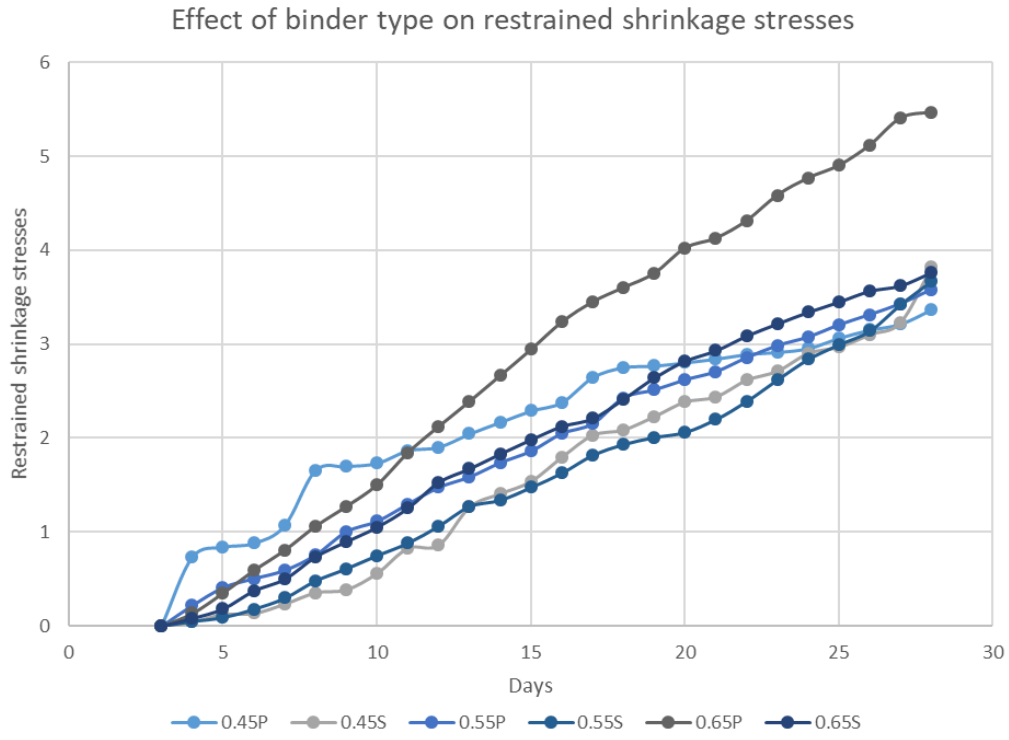

Figure 3. Effect of silica fume on development of restrained shrinkage stresses Stresses

This reduces the Ca/Si in the gel and increases the chain in the gel which improves the elastic properties of the mortar [33,43-45]. The denser matrix created with smaller capillary voids reduced the shrinkage of the mortar as compared to mixes without silica fume. The reduced porosity also leads to a reduction in mass loss and humidity changes in the mortar.

4.3 Effect of shrinkage compensating admixture on development of Restrained Shrinkage Stresses

From Figure 4, shrinkage compensating admixture reduced the development of restrained shrinkage stresses for 0.55 and 0.65 mix. The mix with 0.45 w/c increased restrained shrinkage stresses in 28 days as compared to plain mix.

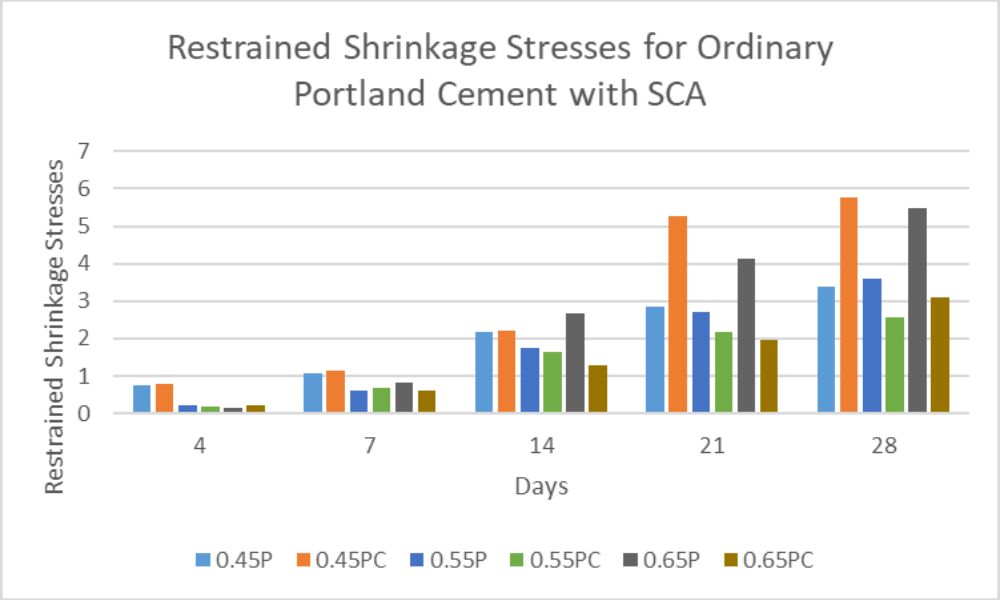

Figure 4. Effect of Shrinkage Compensating admixture on development of Restrained Shrinkage Stresses on Ordinary Portland Cement

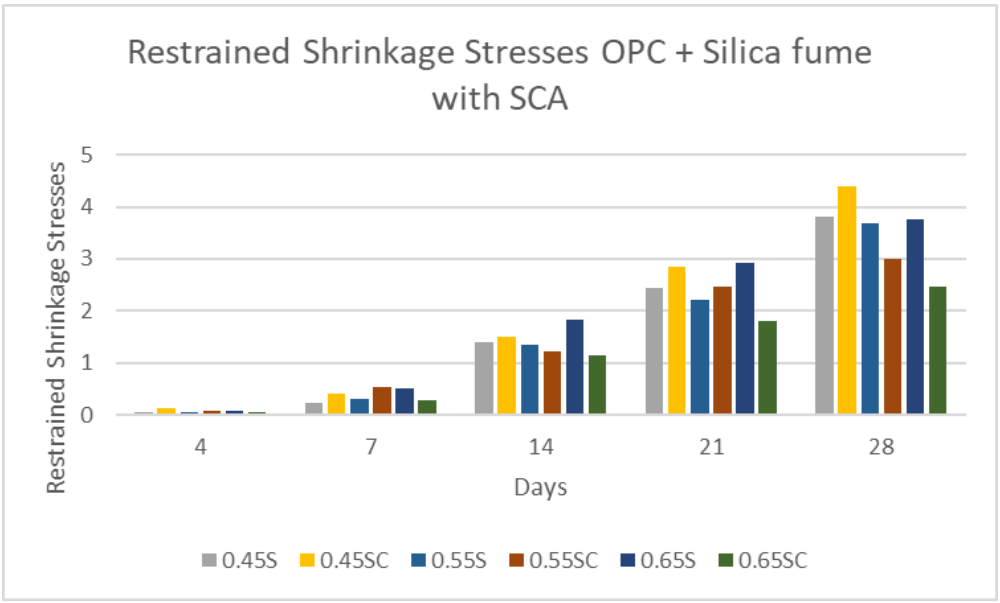

Figure 5. Effect of Shrinkage Compensating admixture on Development of Restrained Shrinkage Stresses on Ordinary Portland Cement with partial replacement with 10% Silica fume.

In Figure 5 in the early days, it was observed that restrained shrinkage stresses were lowest with mixes with silica fume as compared to plain ordinary Portland cement mixes. In 28 days, the highest restrained shrinkage stresses were 0.65, 0.45 and 0.55 mix.

The hydration of shrinkage compensating admixture results in a paste that increases in volume as compared to Portland cement alone. Shrinkage compensating admixtures have an expansive effect that overcomes the shrinkage of Portland cement. In the presence of water there is the formation of ettringite /calcium sulfoaluminate that leads to the expansion reducing drying shrinkage.

While the formation of ettringite may be harmful to mortar in large quantities, the controlled formation of the ettringite leads to a shrinkage compensating effect [46, 47]. Mixes with silica fume generally performed better during early age as compared to plain ordinary Portland cement mixes. This can be explained by the formation of ettringite and the pore filling effect.

4.4 Artificial Neural Network/methodology

In civil engineering, researchers have increasingly embraced the application of machine learning algorithms to address regression problems and analytical modeling challenges. These algorithms have proven valuable in understanding various concrete properties, including structural health monitoring,

compressive strength prediction, concrete mix designs, and material behavior modeling [48-50].

Machine learning models utilized for regression purposes encompass a range of algorithms such as linear regression, gradient boosting, K-means, support vector machines, neural networks, principal component analysis, and random forests, among others. By leveraging these advanced techniques, researchers are gaining deeper insights into the complexities of concrete behavior and properties, contributing to more precise and efficient solutions in civil engineering applications.

Artificial neural networks have garnered global recognition for their remarkable capacity to efficiently solve complex engineering problems with high accuracy. These networks draw inspiration from the human brain's functioning, particularly its nonlinearity, which enables them to comprehend intricate relationships between input variables and the output, as well as its parallelism, allowing simultaneous processing of multiple neurons. The ability of artificial neural networks to emulate these characteristics empowers them to excel in handling challenging engineering tasks, making them a sought-after tool in the field.

An artificial neural network (ANN) utilizes supervised learning to establish relationships between neurons (computing units) and predict the behavior of the property under consideration. The ANN's architecture, comprising input layer, neurons, hidden layers, output layer, and activation function, provides mapping capabilities, enabling it to comprehend system dynamics [51]. Unlike traditional methods, ANN does not necessitate parametric assumptions based on the provided data, rendering it superior in predicting the response variable. For successful application in predicting restrained shrinkage stresses, an in-depth understanding of the influence of various concrete material properties on the development of such stresses is essential. By leveraging ANN's versatility and non-parametric nature, accurate predictions of restrained shrinkage stresses can be achieved, making it a valuable tool in concrete engineering.

The feedforward neural network trained with a backpropagation algorithm reduces the inaccuracy of artificial neural network models. Backward propagation is adopted to adjust the weights and therefore ensure a global optimum is achieved [48]. The multilayer perceptron uses the feedforward and backpropagation algorithms where every input neuron is multiplied by an approximate weight and the product between the input and the weight is activated by an activation function to form an output, which can be described from Equation (13) and Equation 18.

$$u_k = \sum(w_{km} * x_n) \quad (13)$$

$$y_k = f(u_k + b_k) \quad (14)$$

Where x_1, x_2, x_3…. xn are the predictor variables, wk_1, wk_2, wk_3…w_{km} are the weights assigned to the neurons, b_k represents the bias for the neuron k and the function is activated by activation function f, y_k represents the response variable [52].

The activation functions in a neural network are sigmoid functions, rectified linear unit, hyperbolic tanh, and leaky rectified linear unit. The activation functions activate the network to produce predicted response variable y that is approximately close to the measured or observed value y.

4.5 Restrained Shrinkage Stresses Architecture

The architecture of an artificial neural network is tailored to suit the specific engineering problem it addresses. The optimal parameters of the network are determined by the application it serves. To achieve the best performance, hyperparameters are carefully selected through trial and error, with a focus on the optimization function and the optimizer. While too few neurons may be inadequate for educational and training purposes, many neurons can increase computational time, making it less advisable [54].

For this study, a dataset comprising 300 data points obtained from experimental work was utilized. The dataset was split into three sets: 80% for training, 10% for testing, and 10% for validation. The neural network was constructed using Python, an open-source software, to enable flexibility and customization. To evaluate the prediction model's efficacy, predicted values were compared against actual values, ensuring minimal errors.

The research involved developing three distinct models: one for restricted shrinkage stresses of ordinary Portland cement, another for restricted shrinkage stresses with silica fume as a partial replacement, and a third model that combined both scenarios. To successfully settle on the architecture of ANN, manual manipulation of hyperparameters in the model was done with information derived from the literature. The architecture of ANN is shown in Figure 6. The ANN was created by varying the activation functions and the optimization function with a total of 64 neurons. The activation functions varied for the hidden layer were identity, tanh, Relu and logistic sigmoid [54-55].The equations governing the activation functions are as shown in Equation (15), Equation (16), Equation (17) and Equation (18).

Identity $f(x) = x$ (15)

Logistic sigmoid $f(x) = \frac{1}{1+(\exp(-x))}$ (16)

Tanh $f(x) = \tanh(x)$ (17)

Relu $f(x) = \max(0, x)$ (18)

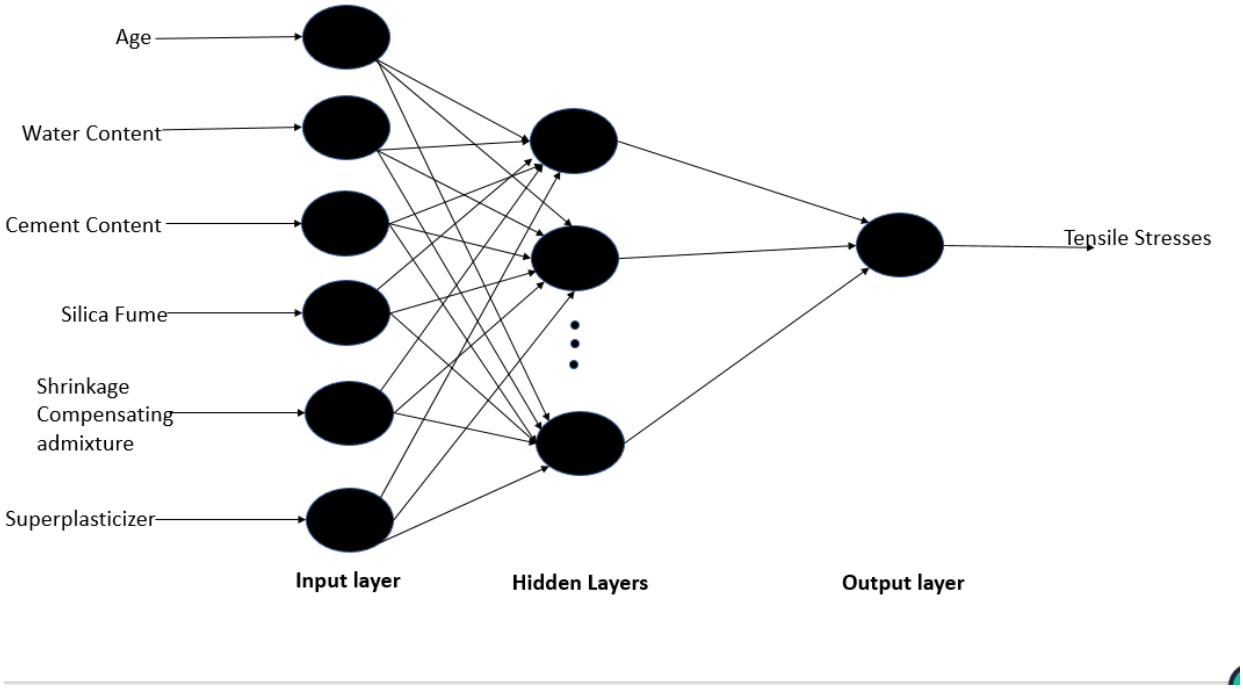

Figure 6. Artificial Neural network model

During the training process, the optimization function was carefully selected through trial and error. Three options were considered: RMSprop, stochastic gradient descent, and the Adam-stochastic gradient optimizer as proposed by Kingma & Ba [55].

For the research, a single hidden layer was utilized. The activation functions applied in this layer were rectified linear unit, hyperbolic tanh, and sigmoid function. To update the weights effectively, different learning rates were experimented with. Three approaches were tested: constant learning rate, where the rate remains fixed throughout training, invscaling learning rate, where the rate decreases after each epoch, and adaptive learning rate, where the rate is maintained constant if the loss function is decreasing. The appropriate model was chosen by cross validating the performance metrics of various models [56].

4.6 Performance of Shrinkage Stresses ANN models

The model's accuracy was evaluated using several performance metrics: coefficient of determination (R2), mean absolute error (M.A.E.), mean absolute percentage error (M.A.P.E.), and root mean squared error (R.M.S.E.). These metrics have been utilized by previous researchers [6, 50, 52]. The coefficient of determination (R2) quantifies the overall variation between predicted and actual values, with a range of 0 to 1. A value of 1 indicates a very strong relationship between the two. The root mean squared error (R.M.S.E.) measures the error between predicted and observed values. However, R.M.S.E. tends to heavily penalize outliers, and it is therefore recommended to complement it with other accuracy metrics, such as the coefficient of determination and Willmot's index of agreement [57]. The metrics can be defined mathematically, as shown in Equation (19) - Equation (22).

$$\boldsymbol{R.M.S.E} = \sqrt{\frac{\sum_{i=1}^{n}(\boldsymbol{T_i}-\boldsymbol{O_i})^2}{\boldsymbol{n}}} \quad (19)$$

$$\boldsymbol{R^2} = \boldsymbol{1} - \frac{\sum_i(\boldsymbol{T_i}-\boldsymbol{O_i})^2}{\sum_i(\boldsymbol{O_i})^2} \quad (20)$$

$$M.A.E = \frac{1}{n}\sum_i^n \parallel T_i - O_i \parallel \quad (21)$$

$$M.A.P.E = \frac{1}{n}\sum_{i=1}^{n}(\frac{O_i-T_i}{O_i}) * 100 \quad (22)$$

Where: O_i is the measured tensile stresses, T_i is the predicted tensile stresses and n is the number of observations.

5. Artificial Neural Network Model Development

5.1 Statistical summary

300 datasets were acquired from the experiment and classified into three primary scenarios based on the binder type. Scenario 1 represented experimental data from concrete mixes that used ordinary Portland cement as a binder. Scenario 2 consisted of data from concrete mixes with 10% silica fume as a partial replacement for ordinary Portland cement. Scenario 3 comprised a combination of data from Scenario 1 and 2.

The tables below present the count, mean, standard deviation, minimum, 25th percentile, 50th percentile (median), 75th percentile, and maximum values for each scenario. The statistics of the data are as shown in **Error! Reference source not found.** for

Scenario 1, Table 4 for Scenario 2 and, Table 5 for Scenario 3.

Table 3. Statistics of Data for Scenario 1: Ordinary Portland Cement as Binder

	Count	mean	Std	min	25%	50%	75%	max
Water content	150	185	4.096	180	180	185	190	190
Cement content	150	342.667	44.491	292	292	336	400	400
Silica fume	150	0	0	0	0	0	0	0
Superplasticizer	150	1.439	0.187	1.226	1.411	1.411	1.68	1.68
SCA	150	0.076	0.0784	0	0	0	0.151	0.18
Age	150	16	7.235	10	16	16	22	28
Remaining stresses	150	3.043	2.076	1.515	2.572	2.572	4.292	8.583

Table 4. Statistics for the data set for Scenario 2: Ordinary Portland Cement + 10% Silica fume

	Count	mean	Std	min	25%	50%	75%	max
Water content	150	185	4.096	180	180	185	190	190
Cement content	150	308.4	40.042	262.8	262.8	302.4	360	390
Silica fume	150	34.267	4.449	29.2	29.2	33.6	40	40
Superplasticizer	150	1.439	0.187	1.226	1.226	1.411	1.68	1.68
SCA	150	0.076	0.0784	0	0	0.0657	0.151	0.18
Age	150	16	7.235	4	10	16	22	28
Remaining stresses	150	1.604	1.239	0.6002	0.6002	1.366	2.259	5.745

Table 5. Statistics for the data set for Scenario 3: Both Binders

	Count	mean	Std	min	25%	50%	75%	max
Water content	300	185	4.089	180	185	185	190	190
Cement content	300	325.533	45.606	262.8	292.00	319.2	360	400
Silica fume	300	17.133	17.446	0	0	14.6	33.6	40
Superplasticizer	300	1.439	0.1865	1.226	1.226	1.411	1.68	1.68
SCA	300	0.076	0.0785	0	0	0.0	0.151	0.18
Age	300	16	7.235	4	10	16	22	28
Remaining stresses	300	2.324	1.852	0.006	0.93243	1.887	3.027	8.5826

5.2 Correlation of Inputs: Analysis and Discussion of Heat Maps

5.2.1. Effect of ordinary Portland Cement on Restrained Shrinkage Stresses

The correlation between the inputs and restrained shrinkage stresses was analyzed and visualized through a heatmap, as depicted in Figure 7. In this correlation heat map, the values range from -1 to 1, representing different types of correlations. A value of -1 indicates a negative correlation, where an increase in the input variable results in a decrease in the response variable, and vice versa. A value of 0 indicates no correlation, while a value of 1 shows a direct proportional relationship, where an increase in the input variable leads to an increase in the response variable.

Specific correlation values were observed in the analysis. The water content and restrained shrinkage stresses showed a negative correlation with a factor of 0.565, indicating that an increase in water content leads to a decrease in restrained shrinkage stresses. On the other hand, cement content and superplasticizer exhibited a positive correlation with a factor of 0.594, suggesting that an increase in these factors corresponds to an increase in restrained shrinkage stresses. Furthermore, the age of the mortar showed a positive correlation of 0.628 with restrained shrinkage stresses, indicating that as the mortar ages, the restrained shrinkage stresses increase. Also, the inclusion of the shrinkage compensating admixture had a positive correlation factor of 0.016, indicating that its addition leads to an increase in restrained shrinkage stresses.

5.2.2. The Effect of Addition of Silica Fume as Partial Replacement of Ordinary Portland Cement on Development of Restrained Shrinkage Stresses

From Figure 8, the inclusion of silica fume in the mortar mixes significantly alters the correlation dynamics. The age of the mortar exhibited a positive correlation with restrained shrinkage stresses, increasing them by a factor of 0.607. Similarly, an increase in cement content positively affected restrained shrinkage stresses, raising them by 0.398. In contrast, the use of silica fume demonstrated a negative correlation, reducing the development of restrained shrinkage stresses by 0.404. Furthermore, an increase in shrinkage compensating admixture and water content showed negative correlations, leading to reductions in restrained shrinkage stresses by 0.043 and 0.029, respectively.

Restrained shrinkage stresses are a factor of elastic modulus, tensile relaxation, and drying shrinkage. The three material properties are affected by the mix design properties. However, there exists a complex relationship between the effects of the input parameters,which are water content, cement content, and the admixtures present in the mix. This study revealed that an increase in water content, silica fume, and shrinkage compensating admixture resulted in a reduction of the elastic modulus, making the mix less stiff. Silica fume played a crucial role in the hydration reaction by facilitating the formation of additional calcium silicate hydrate, which contributed to the mix's overall strength. Additionally, the ultra-fineness of silica fume caused a micro filler effect, leading to a decrease in the porosity of the mortar mix. This, in turn, affected the mix's permeability, water demand, and overall durability [58].

Previous research by Alsayed had noted that silica fume increased the short-term mechanical properties of concrete, including the elastic modulus, but at higher percentage levels, it resulted in reduced compressive strength and creep [59]. However, the current study found that the combined effect of shrinkage compensating admixture, silica fume, and superplasticizer led to a decrease in the elastic modulus of the mortar mix.

Drying shrinkage plays a critical role in the development of restrained shrinkage stresses, as depicted in Equation (9). The magnitude of drying shrinkage is influenced by material properties within the mortar, such as the presence of silica fume and shrinkage compensating admixture. Notably, mixes containing silica fume exhibited lower drying shrinkage compared to mixes with only ordinary Portland cement, a finding supported by other researchers like Alsayed [59].

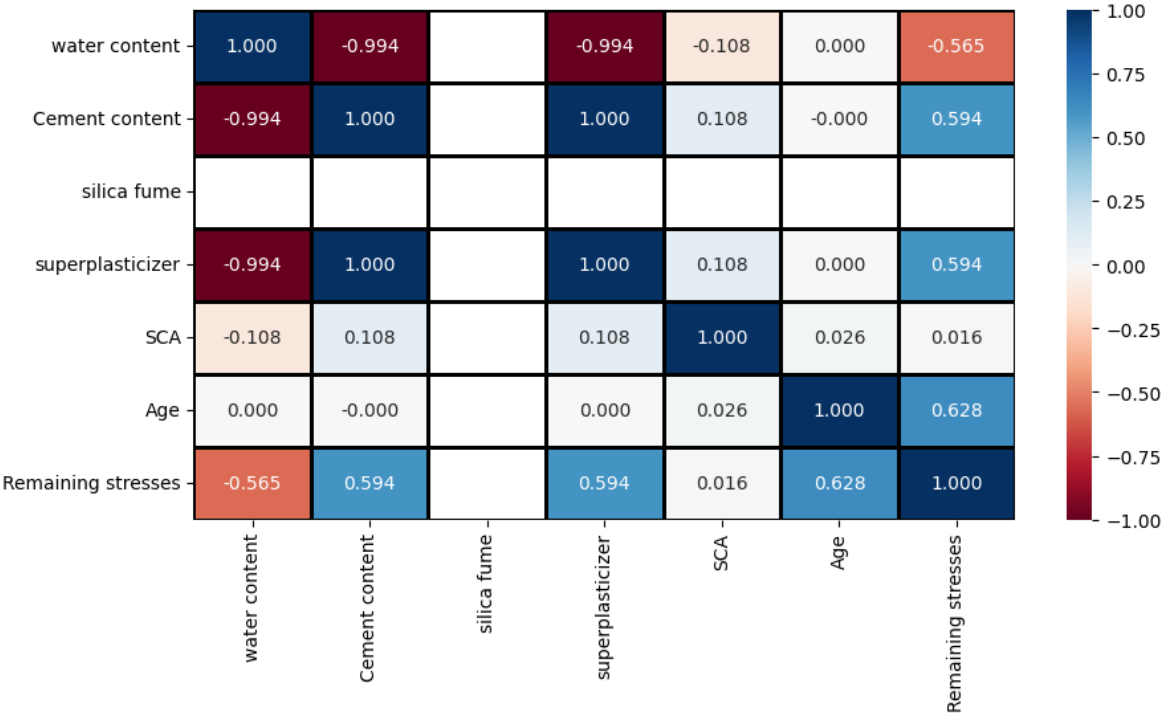

Figure 7. Heat map showing correlaton of input variables on response varible for binder without silica fume

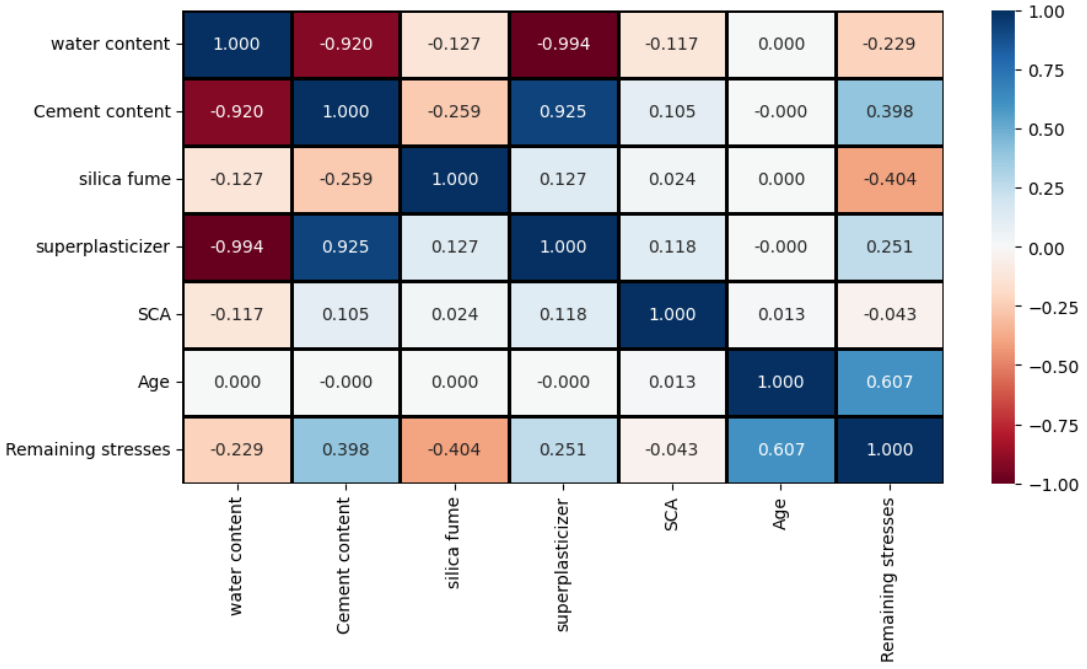

Figure 8. Heat map showing the relationship of the input variables to the restrained shrinkage stresses

The addition of supplementary cementitious materials, such as silica fume, brings about modifications in the mortar's physical and chemical properties due to its filling effect. Given that silica fume possesses finer particles than ordinary Portland cement, it occupies micropores, serving as nucleation sites that promote cement hydration [60]. The hydration process results in the formation of calcium silicate hydrate, thereby increasing the overall density of the mortar's structure. Moreover, the filler effect of silica fume refines larger pores into smaller ones, leading to reduced permeability in the mortar mix [61, 62].

Furthermore, the presence of sand in the mortar mix can contribute to the reduction in permeability by acting as a sink for crystallized calcium hydroxide [63] .The total shrinkage in mortar mixes is influenced by the evaporation of water from the mesopores and macropores present in the C-S-H (calcium-silicate-hydrate) structure [64].The use of supplementary cementitious materials creates a denser matrix structure with smaller capillary voids, which ultimately reduces overall shrinkage. This decrease in porosity also affects the direction of pore distribution, leading to a reduction in mass loss and changes in humidity within the mortar [65].

The study found that the shrinkage compensating admixture exhibited a negative correlation with the development of restrained shrinkage stresses. This admixture is specifically added to mortar mixes to mitigate drying shrinkage. When the shrinkage-compensating admixture is introduced during mixing, it causes an increase in volume due to the formation of ettringite (calcium sulfo aluminate). This ettringite triggers the cement to expand within the initial days, effectively compensating for any potential shrinkage effects [66]. The expansion mechanism operates through various avenues, such as increasing the gel state volume through water adsorption, following the crystal shrinkage-compensation growth theory, or by forming coexisting pores [67].

The development of restrained shrinkage stresses is contingent upon the impact of input parameters on the material properties of the mortar. It is essential to understand the individual effects of each input parameter and how they are influenced by variations in other input parameters to comprehensively grasp their contribution to restrained shrinkage stresses.

5.3 Architecture of Restrained Shrinkage Stresses Neural Network

The development of ANN involved three scenarios based on different binder types with the structures used shown in Table 6, Table 7 and Table 8. Scenario 1 used ordinary Portland cement as the only binder, scenario 2 mixed 10% silica fume as a partial replacement with cement, and scenario 3 combined both binders. In all three scenarios, the ANN structure with the sigmoid activation function achieved the lowest R2 value. The obtained coefficient of determination for scenarios 1, 2, and 3 was 80.21%, 45.57%, and 93.08%, respectively. Using sigmoid and Tanh activation

functions presents a challenge of vanishing gradient, where the model's gradient diminishes as inputs increase or decrease [68]. To address this, the Rectified Linear Unit (Relu) was employed, improving training time.

Table 6. Performance metrics for ANN structures for Scenario 1

Model	No of layers	Activation function	Optimizer	No of neurons	R^2	R.M.S. E	M.A.P. E	M.A. E
A	1	Relu	Sgd	64	0.9942	0.0305	0.0869	0.1392
B	1	Tanh	Sgd	64	0.9965	0.0185	0.0755	0.1088
C	1	Sigmoid	Sgd	64	0.8021	1.0347	0.47	0.7640
D	1	Relu	Adam	64	0.9964	0.0191	0.0401	0.0894
E	1	Tanh	Adam	64	0.9917	0.0432	0.0346	0.1690
F	1	Relu	RMSprop	64	0.9974	0.0138	0.0397	0.0808

Table 7. Perfomance metrics for ANN structure for Scenario 2

Model	No of layers	Activation function	Optimizer	No of neurons	R^2	R.M.S. E	M.A.P.E	M.A.E
A2	1	Relu	Sgd	64	0.9719	0.0338	0.4355	0.1306
B2	1	Tanh	Sgd	64	0.9085	0.1100	0.7986	0.2607
C2	1	Sigmoid	Sgd	64	0.4557	0.6543	1.1987	0.6738
D2	1	Relu	Adam	64	0.9900	0.0120	0.2586	0.0704
E2	1	Tanh	Adam	64	0.9160	0.1010	0.9390	0.2450
F2	1	Relu	RMSprop	64	0.9925	0.0090	0.3161	0.0731

Table 8. Perfomance metrics for ANN structure for Scenario 3

Model	No of layers	Activation function	Optimizer	No of neurons	R^2	R.M.S. E	M.A.P.E	M.A.E
A3	1	Relu	Sgd	64	0.9947	0.0214	0.1382	0.1060
B3	1	Tanh	Sgd	64	0.9904	0.0385	0.1625	0.1517
C3	1	Sigmoid	Sgd	64	0.9308	0.2779	0.8981	0.4160
D3	1	Relu	Adam	64	0.9941	0.0238	0.1697	0.1244
E3	1	Tanh	Adam	64	0.9873	0.0511	0.2362	0.1783
F3	1	Relu	RMSprop	64	0.9977	0.0093	0.1775	0.0804

Across all the 3 scenarios and regardless of the optimizer used, the coefficient of determination (R2) achieved accuracies exceeding 99% when Rectified Linear Unit was used.

Among the optimizers, RMSprop exhibited a slightly higher R2 score compared to Adam and stochastic gradient descent, in a decreasing order. Specifically, the coefficient of determination (R2) for scenarios 1, 2, and 3 was 99.74%, 99.25%, and 99.75%, respectively. Notably, Adam and RMSprop optimizers outperformed stochastic gradient descent due to the latter's tendency to get stuck at local minima, failing to reach the global minimum, and leading to longer convergence times [69].

5.4 Performance Metrics of the Restrained Shrinkage Stresses Models

In the ANN framework, the predicted results were cross validated for the three case scenarios. The restrained shrinkage stresses data for ordinary Portland cement were partitioned into three groups: 80% for training, 10% for testing, and 10% for validation. The total number of experimental data points for this case

was 150, with 120 tests used for the training phase, 15 data sets used for testing, and 15 tests used for validation.

5.4.1. Scenario 1: Mixes with Ordinary Portland Cement as the only Binder

Model F demonstrated the best performance in terms of the performance metrics, achieving a coefficient of determination (R2) of 99.74%. It also had a mean absolute percentage error of 0.0397, a mean absolute error of 0.0808, and a root mean squared error of 0.0138. The ANN structure of model F consisted of one hidden layer, using the rectified linear unit (Relu) as the activation function, and RMSprop as the optimizer.

Based on Figure 9, it is evident that the predicted values closely align with the actual values from the experiment, achieving an impressive accuracy of 99.74%. Consequently, artificial neural networks prove to be effective in predicting restrained shrinkage stresses for mortar mixes using ordinary Portland cement as the binder. Similarly, for all other ANN structures in models A–F, except for model C, the R values exceed 0.9, indicating a substantial relationship between the predicted and actual values [70]. The mean squared error and R2 are metrics used to determine accuracy the low values of RMSE and a high R2 indicate the usefulness of model. Thus, these findings support the use of neural networks for developing accurate predictive models. Hence, it is evident that the ANN architecture utilizing tanh and Relu as activation functions in conjunction with stochastic gradient descent, Adam, and RMSprop optimizers effectively predict restrained shrinkage stresses. The remarkable correlation observed between the actual values and predictions, with minimal error margins, underscores the utility of ANN. Most values closely align with the line of fit, as depicted in the figure below, further validating the accuracy and reliability of the predictive model.

5.4.2. Scenario 2: Mixes with 10% Silica Fume as Partial Replacement.

In scenario 2, where ordinary Portland cement was partially replaced with silica fume, the graph in Figure 10, illustrates that all ANN models, except Model C2 with sigmoid activation function, achieved a coefficient of determination greater than 0.9. The dataset comprised 150 samples, distributed with 80% for training, 10% for validation, and 10% for testing. The value of 0.9 represents the anticipated strong correlation between the predicted and actual values. Notably, Model F2 obtained the highest R score, matching the performance observed in Scenario 1 with ordinary Portland cement as the sole binder. Model F2 achieved an impressive coefficient of determination of 0.9925, alongside a mean absolute percentage error of 0.3161, a mean absolute error of 0.0731, and a root mean squared error of 0. 9925.On the other hand, Model C2 displayed an R2 of 45.57%, indicating low accuracy and unsuitability for predicting restrained shrinkage stresses.

5.4.3 Scenario 3: Combination of Scenario 1 and 2

Scenario 3 involved creating a combined model using data from both binders. The ANN models utilized a dataset of 300 samples, with 80% allocated for training, 10% for testing, and 10% for validation. The graph in the Figure 11, illustrates the predicted versus actual values. Remarkably, regardless of the model structure used, the observed R values consistently exceeded 0.9, indicating a strong relationship between the predicted and actual values.

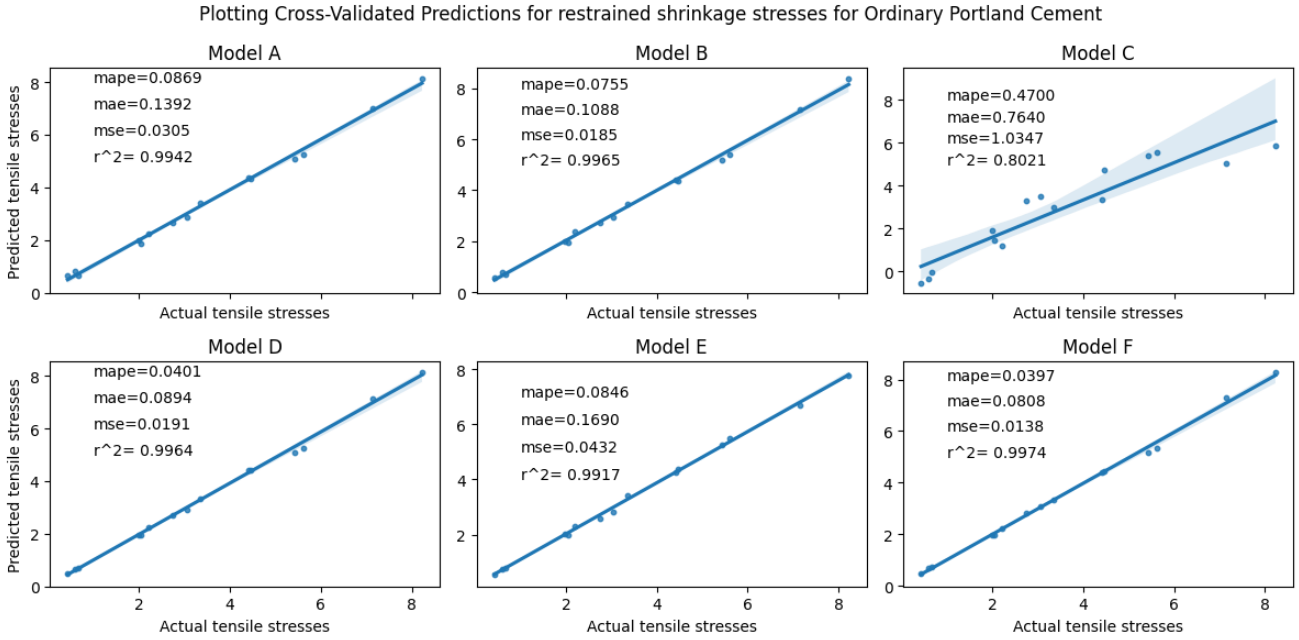

Figure 9. Plotting cross-validated predictions for restrained shrinkage stresses for scenario 1

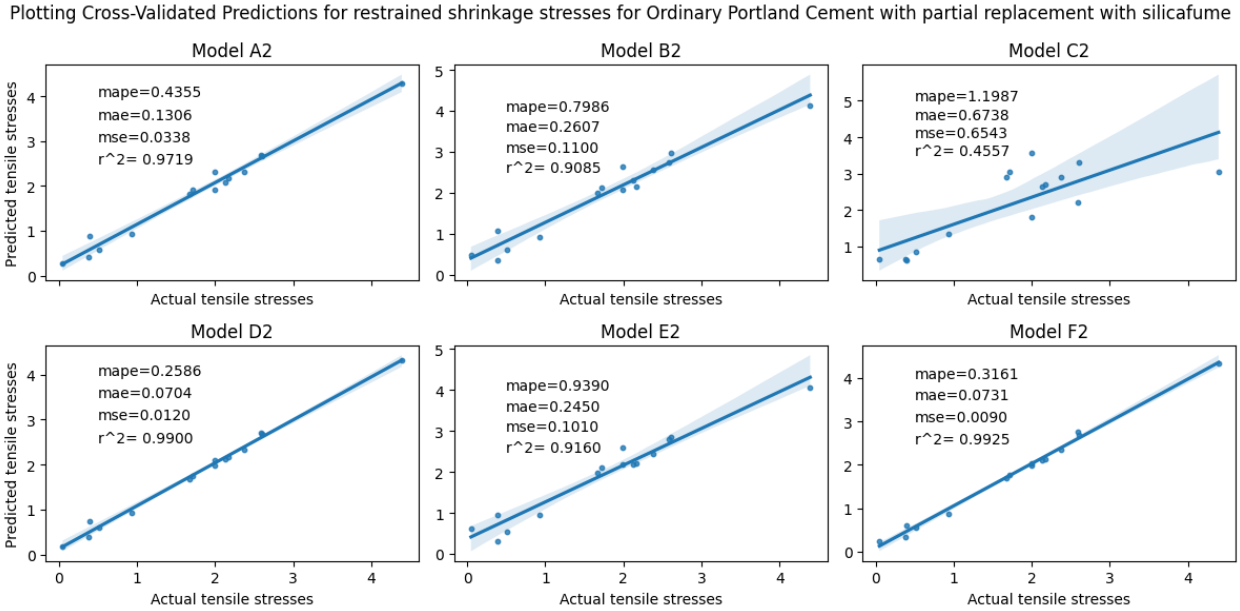

Figure 10. Plotting cross validated Predictions for restrained shrinkage stresses for Scenario 2

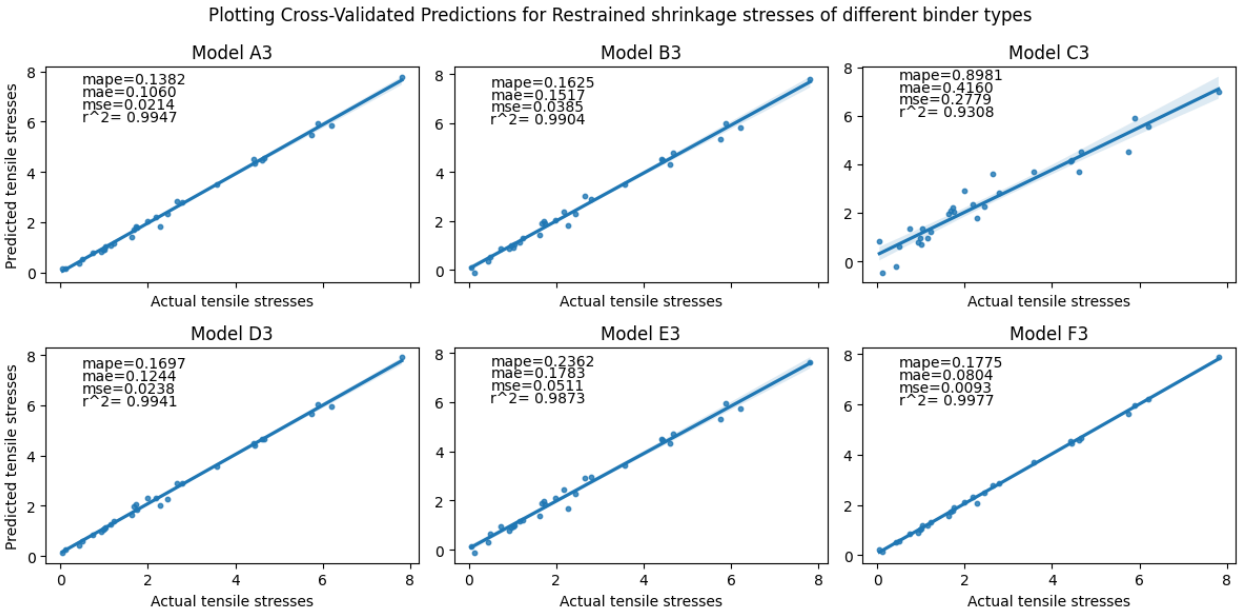

Figure 11. Plotting cross validated predictions for restrained shrinkage stresses for Scenario 3

Notably, Model F3 exhibited the highest performance, achieving a coefficient of determination of 0.9977, a mean squared error of 0.0093, a mean absolute error of 0.0804, and a mean absolute percentage error of 0.1775.

The results demonstrate the effectiveness of Model F3 in accurately predicting restrained shrinkage stresses in scenario 3, and the ANN's robust performance showcases its potential as a powerful tool for such predictions. In the three scenarios the optimum model was selected by choosing the model with the highest coefficient of determination. R squared is a measure of the percentage of total variation of the dependant variable that can be explained by the independent variable. The root mean squared for model F3 in Figure 11 is 0.0093 which indicates the difference between the observed values and the predicted values are very close and therefore the model can accurately fit the data set. The Mean absolute error in Model F2 is 0.0731 which is close to Model D2. The two models have high accuracy metrics and therefore can both be adequate for the model.

5.4.4 Comparison with Traditional Models

The models created using the artificial neural network indicate a better performance with the coefficient of determination for different binders being 99.77% which is higher than traditional models. An analysis of the performance of the previous models was previously done by Kristiawan [25]. The research observed that the model made from prestressed anology theory by Silferbrand [21] had a coefficient of regression of 85% from the measured values, the model by proposed by Denarie et al. [23] had an accuracy of 59.95%, model proposed by had an accuracy of 75%. The model developed is therefore 14% higher than the model by Silferbrand [21],39.82% higher than the model by Denarie et al. [23], and 24.77% higher than the model by Baluch which were developed using the material property theory. The research can therefore observe that the model is more robust and versatile than traditional analytical models.

5. Conclusions

This study employed artificial neural networks (ANNs) to predict restrained shrinkage stresses in different binder types. The ANN models considered key input parameters, including age, ordinary Portland cement, silica fume, water content, superplasticizer, and shrinkage compensating admixture. The dataset comprised 300 samples, leading to the development of three distinct ANN models. The optimal ANN structure consisted of one hidden layer with 64 neurons, utilizing the rectified linear unit as the activation function, and employing RMSprop as the optimizer.

For mortars with ordinary Portland cement as the sole binder, the ANN model achieved remarkable results with R values, mean absolute error (MAE), mean absolute percentage error (MAPE), and root mean square error (RMSE) of 99.74%, 0.0808, 0.0397, and 0.0138, respectively. Similarly, in mortars containing partial replacement of cement with silica fume, the ANN model exhibited satisfactory performance, yielding R values, MAE, MAPE, and RMSE of 99.25%, 0.0090, 0.0731, and 0.3161, respectively. Furthermore, when datasets for both binder types were combined, the ANN model yielded R values, MAE, MAPE, and RMSE of 99.77%, 0.0093, 0.0804, and 0.1775, respectively.

The study revealed that artificial neural networks can effectively predict restrained shrinkage stresses in mortars, regardless of the binder type. The coefficient of determination ratios was nearly close to one, indicating significant accuracy of the developed models when compared to actual values. Significant correlations were identified between restrained shrinkage stresses and the input parameters. Cement content, age, and superplasticizer exhibited positive correlations, while silica fume, water content, and shrinkage compensating admixture displayed negative correlations.

In conclusion, the utilization of artificial neural networks is a valuable approach for accurately predicting restrained shrinkage stresses in repair mortars. These findings contribute to understanding the key factors influencing restrained shrinkage stresses and offer insights into optimizing the performance and durability of repaired concrete structures. Future research should explore additional parameters and expand the application of ANN models to further enhance their predictive capabilities in diverse mortar compositions.

References

[1] Z. Li, (2011) Advanced Concrete Technology. Wiley Online Library. https://doi.org/10.1002/9780470950067

[2] H. Beushausen, M. Chilwesa, Assessment and prediction of drying shrinkage cracking in bonded mortar overlays. Cement and Concrete Research, 53 (2013) 256–266. https://doi.org/10.1016/j.cemconres.2013.07.008

[3] A.M. Vaysburd, B. Bissonnette, K. F. von Fay, (2014). Compatibility issues in design and implementation of concrete repairs and overlays. US Department of the Interior, Bureau of Reclamation, Technical Service Center, Materials Engineering and Research Laboratory.

[4] H. Beushausen, M.G. Alexander, Localised strain and stress in bonded concrete overlays subjected to differential shrinkage. Materials and Structures/Materiaux et Constructions, 40(2), 189–199. https://doi.org/10.1617/s11527-006-9130-z

[5] T. Dittmer, H. Beushausen, The effect of coarse aggregate content and size on the age at cracking of bonded concrete overlays subjected to restrained deformation. Construction and Building Materials, 69 (2014) 73–82. https://doi.org/10.1016/j.conbuildmat.2014.06.056

[6] D.R. Nayak, R.R. Pattnaik, B. Chandra Panda, Study on relative shrinkage of cement-based micro-concrete for durable concrete repair. Cleaner Engineering and Technology, 8, (2022). https://doi.org/10.1016/j.clet.2022.100444

[7] D.P. Bentz, W.J. Weiss, Quantifying Stress Development and Remaining Stress Capacity in Restrained, Internally Cured Mortars. ACI Materials Journal, 110(1), 3-11.

[8] D.A. Lange, H.C. Shin, Early age stresses and debonding in bonded concrete overlays. Transportation research record, 1778(1), (2001) 174-181. https://doi.org/10.3141/1778-21

[9] S. Sajedi, F. Ghassemzadeh, I. Harsini, M. Shekarchi, B. Mohammadi, Behavior of bonded concrete overlays under restrained shrinkage.

First Middle East Conference on Samrt Monitoring Assessment and Rehabilitation of Civil Structures, Dubai.

[10] A. Bentur, K. Kovler, Evaluation of early age cracking characteristics in cementitious systems. Materials and Structures, 36 (2003) 183–190. https://doi.org/10.1007/BF02479556

[11] N. Banthia, R. Gupta, Plastic shrinkage cracking in cementitious repairs and overlays. Materials and Structures/Materiaux et Constructions, 42(5), 567–579. https://doi.org/10.1617/s11527-008-9403-9

[12] W.J. Weiss, W. Yang, S.P. Shah, Shrinkage Cracking of Restrained Concrete Slabs. Journal of Engineering Mechanics, 124(7), (1998) 765–774. https://doi.org/10.1061/(ASCE)0733-9399(1998)124:7(765)

[13] I. Khan, A. Castel, R.I. Gilbert, Tensile creep and early-age concrete cracking due to restrained shrinkage. Constr Build Mater, 149, (2017) 705–715. https://doi.org/10.1016/j.conbuildmat.2017.05.081

[14] R.D. Toledo Filho, K. Ghavami, M.A. Sanjuán, G.L. England, Free, restrained and drying shrinkage of cement mortar composites reinforced with vegetable fibres. Cement and Concrete Composites, 27(5), (2005) 537–546. https://doi.org/10.1016/j.cemconcomp.2004.09.005

[15] P. Lv, G. Long, Y. Xie, J. Peng, S. Guo, Study on the mitigation of drying shrinkage and crack of limestone powder cement paste and its mechanism. Construction and Building Materials, 411, (2024) 134325. https://doi.org/10.1016/j.conbuildmat.2023.134325

[16] J.E. Rossen, B. Lothenbach, K.L. Scrivener, Composition of C-S-H in pastes with increasing Levels of silicafume addition. Cement and Concrete Research, 75, (2015) 14-22. https://doi.org/10.1016/j.cemconres.2015.04.016

[17] F. Azarhomayun, M. Haji, M. Kioumarsi, M. Shekarchi, Effect of calcium stearate and aluminum powder on free and restrained drying shrinkage, crack characteristic and mechanical properties of concrete. Cement and Concrete Composites, 125, (2022) 104276. https://doi.org/10.1016/j.cemconcomp.2021.104276

[18] H. Beushausen, M. Gillmer, The use of superabsorbent polymers to reduce cracking of bonded mortar overlays. Cement and Concrete Composites, 52, (2014) 1–8. https://doi.org/10.1016/j.cemconcomp.2014.03.009

[19] Y.S. Yuan, Restrained shrinkage in repaired reinforced concrete elements. Materials and Structures, 27, (1994) 375–382. https://doi.org/10.1007/BF02473440

[20] Y. Yuan, G. Li, and Y. Cai, Modeling for prediction of restrained shrinkage effect in concrete repair. Cement and concrete research, 33(3), (2003) 347-352.

[21] J. Silfwerbrand, Bonded concrete overlays for repairing concrete structures. in Failure, Distress and Repair of Concrete Structures, Elsevier Ltd, (2009) 208–243. https://doi.org/10.1533/9781845697037.2.208

[22] M.H. Baluch, M.K. Rahman, A.H. Al-Gadhib, Risks of Cracking and Delamination in Patch Repair. Journal of Materials in Civil Engineering,14(4), 294–302. https://doi.org/10.1061/(ASCE)0899-1561(2002)14:4(294)

[23] E. Denarie, J. Silfwerbrand, H. Beushausen, (2011) Bonded Cement-Based Material Overlays for the Repair, the Lining or the Strengthening of Slabs or Pavements. RILEM State of the Art Reports, Springer Netherlands.

[24] J. Carlswärd, (2006) Shrinkage cracking of steel fibre reinforced self-compacting concrete overlays: test methods and theoretical modelling. Dissertation, Lulea University of Technology, Lulea, Sweden,

[25] S.A. Kristiawan, Performance criteria to assess shrinkage cracking tendency in concrete overlay. Procedia Engineering, Elsevier Ltd, 54, (2013) 82–100. https://doi.org/10.1016/j.proeng.2013.03.008

[26] H. Beushausen, A parameter study on the age at cracking of bonded concrete overlays subjected to restrained shrinkage. Materials and Structures/Materiaux et Constructions, 49(5),1905–1916. https://doi.org/10.1617/s11527-015-0622-6

[27] M. Raupach, Forschung auf dem Gebiet des Bauinstandsetzens – Derzeitige Ansätze und zukünftige Aufgaben / Research in the Field of Repair - Actual Approaches and Future Needs. Restoration of Buildings and Monuments, 15(4), 239–254. https://doi.org/10.1515/rbm-2009-6303

[28] N.R.J. Baldwin, E.S. King, (2003). Field Studies of the Effectiveness of Concrete Repairs: Phase 4 Report: Analysis of the Effectiveness of Concrete Repairs and Project Findings. Health and Safety Executive.

[29] ASCE, (2009), 2009 Report Card/or America's Infrastructure. Washington DC.

[30] K. Kuder, J. Berman, G. Hannesson, and R. Shogren, Mechanical Properties of Self Consolidating Concrete Blended with High Volumes of Fly Ash and Slag. Construction and

Building Materials, 34, (2012) 285–295. https://doi.org/10.1016/j.conbuildmat.2012.02.034

[31] M.A. Megat Johari, J.J. Brooks, S. Kabir, P. Rivard, Influence of supplementary cementitious materials on engineering properties of high strength concrete. Construction and Building Materials, 25(5), 2639–2648. https://doi.org/10.1016/j.conbuildmat.2010.12.013

[32] P. Chindaprasirt, C. Jaturapitakkul, T. Sinsiri, Effect of lfyash on compressive strength and pore size refinement of blended cement paste. Cement and Concrete Composites, 27(4), (2005) 425–428. https://doi.org/10.1016/j.cemconcomp.2004.07.003

[33] H.H. Nassif, H. Najm, N. Suksawang, Effect of pozzolanic material and curing methods on the Elastic Modulus of HPC. Cem Concr Compos, 27(6), (2004) 661–670. https://doi.org/10.1016/j.cemconcomp.2004.12.005

[34] C136 Standard Test Method for Sieve Analysis of Fine and Coarse Aggregates. Accessed: Feb. 12, 2024. [Online]. Available: https://www.astm.org/standards/c136

[35] BS 8110-1-1997, "Structural use of concrete-Part 1: Code of practice for design and construction ICS 91.080.40," British Standard (BSI), vol. 2, pp. 1–168, 2005.

[36] BS 8110-1-1997, Structural use of concrete-Part 1: Code of practice for design and construction British Standard (BSI), 2, (2005) 1–168.

[37] "C157 Standard Test Method for Length Change Of Hardened Cement Mortar And Concrete." Accessed: Feb. 14, 2024. [Online]. Available: https://www.astm.org/standards/c157

[38] K.R. Kordina, G. Mancini, K. Schäfer, A. Schieβl, K. Zilch, fib Bulletin 54. Structural Concrete Textbook on behaviour, design and performance Second edition Volume 4," Oct. 2010, https://doi.org/10.35789/fib.BULL.0055

[39] "BS EN 1992 - Eurocode 2. Design of concrete structures." Accessed: Feb. 12, 2024. [Online].

[40] W. Wang, J. Gong, New relaxation function and age-adjusted effective modulus expressions for creep analysis of concrete structures. Engineering Structures, 188, (2019) 1-10. https://doi.org/10.1016/j.engstruct.2019.03.009

[41] Y.Y. Kim, K.M. Lee, J.W. Bang, S. J. Kwon, Effect of W/C ratio on durability and porosity in cement mortar with constant cement amount. Advances in Materials Science and Engineering, 2014, (2014). https://doi.org/10.1155/2014/273460

[42] S. Shahbazpanahi, M.K. Tajara, R.H. Faraj, A. Mosavi, Studying the C–H crystals and mechanical properties of sustainable concrete containing recycled coarse aggregate with used nano-silica. Crystals (Basel), 11(2), (2021) 122. https://doi.org/10.3390/cryst11020122

[43] S. Fallah, M. Nematzadeh, Mechanical properties and durability of high strength concrete containing macropolymeric and polypropylen fibres with nnanosilica and silica fume. Construction and Building Materials, 132, (2016) 170–187. https://doi.org/10.1016/j.conbuildmat.2016.11.100

[44] Y. Li, Y. Liu, R. Wang, Evaluation of the elastic modulus of concrete based on identation test and multi-scale homogenization method. Journal of Building Engineering,43, (2021) 102758. https://doi.org/10.1016/j.jobe.2021.102758

[45] A.C. Muller, K.L. Scrivener, J. Skibsted, A.M. Gajewicz, P.J. McDonald, influence of silica fume on the microstructure of pastes. Cement and Concrete Research, 74 (2015) 116–125. https://doi.org/10.1016/j.cemconres.2015.04.005

[46] J.J. Brooks, Shrinkage of Concrete. Concrete and Masonry Movements, (2015)137–185. https://doi.org/10.1016/B978-0-12-801525-4.00006-6

[47] M. Collepardi, A. Borsoi, J.J. Olagot, R. Troli, Effects of shrinkage compenating concrete unde non-wet curing conditions. Cement and Concrete Composites, (2004), 704–708. https://doi.org/10.1016/j.cemconcomp.2004.09.020

[48] P. Alidoust, S. Goodarzi, A. Tavana Amlashi, L. Sadowski, Comparative analysis of soft computing techniques in predicting the compressive and tensile strength of seashell containing concrete. European Journal of Environmental and Civil Engineering, 27(5), (2022) 1853-1875. https://doi.org/10.1080/19648189.2022.2102081

[49] J. Abellán García, J. Fernández Gómez, N. Torres Castellanos, Properties prediction of environmentally friendly ultra-high-performance concrete using artificial neural networks. European Journal of Environmental and Civil Engineering, 26(6), (2022) 2319–2343. https://doi.org/10.1080/19648189.2020.1762749

[50] P. Chopra, R.K. Sharma, M. Kumar, Prediction of Compressive Strength of Concrete Using Artificial Neural Network and Genetic Programming. Advances in Materials Science and Engineering, 2016, (2016). https://doi.org/10.1155/2016/7648467

[51] C.T. Leondes, (2003) Intelligent systems: technology and applications. CRC Press.

[52] S. Kekez, J. Kubica, Application of artificial neural networks for prediction of mechanical properties of cnt/cnf reinforced concrete. Materials, 14(19),

(2021). https://doi.org/10.1155/2016/7648467

[53] A. Ravi Theja, M. Srinivasula Reddy, B.B. Jindal, C. Sashidhar, Predicting the Strength Properties of Self-Healing Concrete Using Artificial Neural Network. Journal of Soft Computing in Civil Engineering, 7(1), (2023) 56–71. https://doi.org/10.1142/5249-vol2

[54] G. Shmueli, P.C. Bruce, M.L. Stephens, N.R. Patel, (2017) Data mining for business analytics: concepts, techniques, and applications, R. John Wiley & Sons.

[55] D.P. Kingma, J.L. Ba, (2015) ADAM:A Method for Stochastic Optimization. Cornell University, arxiv. https://doi.org/10.48550/arXiv.1412.6980

[56] F. Pedregosa, G. Varoquaux, A. Gramfort, V. Michel, B. Thirion, O. Grisel, M. Blondel, P. Prettenhofer, R. Weiss, V. Dubourg, J. Vanderplas, A. Passos, D. Cournapeau, M. Brucher, M. Perrot, E. Duchesnay, Scikit-learn:Machine Learning in Python. Journal of Machine Learning Research, 12, (2011) 2825-2830.

[57] K.O. Achieng, Modelling of soil moisture retention curve using machine learning techniques: Artificial and deep neural networks vs support vector regression models. Computers & Geosciences, 133, (2019) 104320. https://doi.org/10.1016/j.cageo.2019.104320

[58] B.B. Sabir, (1995) High-strength condensed silica fume concrete. Magazine of Concrete Research, 47(172), 219-226. https://doi.org/10.1680/macr.1995.47.172.219

[59] S.H. Alsayed, Influence of Superplasticizer, Plasticizer, And Silica Fume on The Drying Shrinkage of High-Strength Concrete Subjected to Hot-Dry Field Conditions. Cement and Concrete Research, 28(10), (1998) 1405-1415. https://doi.org/10.1016/S0008-8846(98)00102-1

[60] P. Pipilikaki, M. Katsioti, Study of the hydration process of quaternary blended cements and durability of the produced mortars and concretes. Construction and Building Materials, 23(6), (2009) 2246–2250. https://doi.org/10.1016/j.conbuildmat.2008.11.015

[61] K. Githachuri, M.G. Alexander, Durability performance potential and strength of blended Portland limestone cement concrete. Cement and Concrete Composites, 39, (2013) 115–121. https://doi.org/10.1016/j.cemconcomp.2013.03.027

[62] N. Dave, A.K. Misra, A. Srivastava, A.K. Sharma, S.K. Kaushik, Study on quaternary concrete micro-structure, strength, durability considering the influence of multi-factors. Constr Build Mater, 139, (2017) 447–457. https://doi.org/10.1016/j.conbuildmat.2017.02.068

[63] H. Cheng-Yi, R.F. Feldman, (1985) Hydration reactions in Portland cement-silica fume blends. Cement and Concrete Research, 15(4), 585-592. https://doi.org/10.1016/0008-8846(85)90056-0

[64] M.C. Garci Juenger, H.M. Jennings, Examining the relationship between the microstructure of calcium silicate hydrate and drying shrinkage of cement pastes. Cement and Concrete Research, 32(2), (2002) 289–296. https://doi.org/10.1016/S0008-8846(01)00673-1

[65] Z. Wan, T. He, N. Chang, R. Yang, H. Qiu, Effect of silica fume on shrinkage of cement-based materials mixed with alkali accelerator and alkali-free accelerator. Journal of Materials Research and Technology, 22, (2023) 825–837. https://doi.org/10.1016/j.jmrt.2022.11.110

[66] M. Liska, A. Wilson, J. Bensted, Special Cements, Lea's Chemistry of Cement and Concrete, (2019) 585–640. https://doi.org/10.1016/B978-0-08-100773-0.00013-7

[67] S. Nagataki, H. Gem, (1998) Expansive admixtures (mainly ettringite). Cement and Concrete Composites, 20(2-3), 163-170. https://doi.org/10.1016/S0958-9465(97)00064-4

[68] H. Il Suk, An Introduction to Neural Networks and Deep Learning. Deep Learning for Medical Image Analysis, (2017) 3–24. https://doi.org/10.1016/B978-0-12-810408-8.00002-X

[69] E. Hassan, M.Y. Shams, N.A. Hikal, S. Elmougy, The effect of choosing optimizer algorithms to improve computer vision tasks: a comparative study. Multimedia Tools and Applications, 82, (2022) 16591–16633. https://doi.org/10.1007/s11042-022-13820-0

[70] P. Manikandan, V. Vasugi, Potential utilization of waste glass powder as a precursor material in synthesizing ecofriendly ternary blended geopolymer matrix. Journal of Cleaner Production, 355, (2022) 131860. https://doi.org/10.1016/j.jclepro.2022.131860

Authors Contribution Statement

MWN: Conceptualization, MWN, SOA, EKK, KOA: Methodology, Data Curation& Data Analysis MWN, KOA: Software and Modelling. All authors participated in the writing, editing and review of the article.

Funding

The authors declare that no funds, grants or any other support were received during the preparation of this manuscript.

Data Availability

The data supporting the findings of this study can be obtained from the corresponding author upon reasonable request.

Has this article screened for similarity?

Yes

Competing Interests

The authors declare that there are no conflicts of interest regarding the publication of this manuscript.

About the License